Available online at www.sciencedirect.com
SCIENCE DIRECT
Polymer 47 (2006) 1620–1629
polymer
www.elsevier.com/locate/polymer

# Crystallization behavior of polymer/montmorillonite nanocomposites. Part II. Intercalated poly(ε-caprolactone)/montmorillonite nanocomposites

Douwe Homminga [a], Bart Goderis [a], Igor Dolbnya [b], Gabriel Groeninckx [a,*]

[a] *Division of Molecular and Nanomaterials, Laboratory of Macromolecular Structural Chemistry, Department of Chemistry, Catholic University of Leuven (KULeuven), Celestijnenlaan 200F, Heverlee 3000, Belgium*
[b] *Dubble CRG/ESRF, c/o BP 220, Grenoble Cedex F38043, France*

Received 25 March 2005; received in revised form 16 November 2005; accepted 23 December 2005
Available online 19 January 2006

**Abstract**

The combination of surfactant modified montmorillonite (MMT) silicate layers, poly(ε-caprolactone) (PCL) and the adopted melt processing procedure results in intercalated nanocomposites in which the silicate layers act as nucleating agents for the crystallization of the PCL matrix and by which in turn the overall crystallization rate increases. At a sufficiently high MMT concentration and degree of supercooling the polymer-swollen silicate layer stacks disturb crystal growth, resulting in a decrease in the overall crystallization rate. Simultaneous, time resolved, synchrotron small and wide angle X-ray scattering experiments reveal that—when the retarding effect is absent at a sufficiently high temperature—the final semicrystalline structures of pure PCL and its nanocomposites are identical. The poorer nucleation in the case of pure PCL, however, results in a time wise smearing of primary and secondary crystallization whereas in the nanocomposites these events are well separated due to a nucleation induced, efficient and rapid primary crystallization. Secondary crystallization involves the insertion of new lamellar crystals in between the already existing ones.


*Keywords:* Poly(ε-caprolactone); Nanocomposite; Nucleating agent

## 1. Introduction

Nanocomposites based on polymers and layered silicates have attracted much attention in the last decade. Polymer layered silicate nanocomposites (PLSN) show a considerable enhancement of strength, modulus, gas barrier resistance and heat distortion temperature compared to their pure polymer counterparts [1–7], even with silicate loadings as low as 1–4 vol%. Moreover, PLSN are also interesting from the fundamental point of view due to the nano-scale constraints of the filler to the polymer matrix and the ultra-large specific interfacial area between the silicate and the polymer matrix.

Two types of PLSN are known: intercalated and exfoliated nanocomposites. In the former case the polymer chains are inserted between the silicate layers, thereby increasing the silicate layer interlayer distance of the stacks of the original clay structure without destroying them. In the exfoliated case the silicate layers are uniformly dispersed over the polymer matrix and the stacks of the original clay structure are delaminated.

In most PLSN crystallization studies, the polymer matrix was either polyamide-6 (PA-6) or polypropylene (PP) [3,6,8–16]. In the case of PA-6 nanocomposites, the main focus has been on the influence of the silicate layers on the polymorphic crystal structures of PA-6. Recently, polyethylene oxide (PEO) systems were also considered [17]. Silicate type minerals, like talc and mica, are well-known nucleating agents [18,19] and it has been reported that the nano-sized silicate layers too act as nucleating agents in the crystallization of the polymer matrix of PLSN, resulting in higher crystallization rates [3,6,8–16]. On the other hand, lower crystallization rates have also been reported—in particular at relatively high silicate loadings—and associated with a reduction of the polymer crystal growth rate [17,20–23]. During the crystallization of the matrix polymer, the silicate layers act as non-crystallisable barriers that disturb or completely stop crystal growth. Another possibility is that the silicate layers hindrance polymer chain motion, required for crystallization [17,20]. Lincoln et al. also mentioned that the reduced mobility of polymer chains through

* Corresponding author. Tel.: +32 16 327440; fax: +32 16 327990.
*E-mail address:* gabriel.groeninckx@chem.kuleuven.ac.be (G. Groeninckx).

0032-3861/$ - see front matter © 2006 Elsevier Ltd. All rights reserved.
doi:10.1016/j.polymer.2005.12.080

nanoscale constraints caused by silicate layers can have a profound effect on the crystallization process [3].

In the present study poly(ε-caprolactone) (PCL) serves as the matrix polymer. PCL is a biodegradable aliphatic polyester known for its use in medical devices, pharmaceutical controlled release systems and in biodegradable packaging [24]. PCL is a crystallisable polymer with a crystallinity around 45%, a glass-transition temperature of −64 °C [25] and a melting temperature of 60 °C.

This study aims at unraveling the influence of the silicate layers, i.e. montmorillonite (MMT), on the semicrystalline PCL morphology development. Several PCL/MMT nanocomposites were prepared by melt-extrusion with MMT contents of 1, 2, 4 and 10 wt%, respectively. The silicate morphology of the PCL/MMT nanocomposites was identified by X-ray diffraction and transmission electron microscopy. Differential scanning calorimetry (DSC) was used to follow the evolution of the mass faction crystallinity. The development of the PCL semicrystalline lamellar structure was investigated by using time resolved synchrotron small-angle (SAXS) and wide-angle X-ray scattering (WAXS).

## 2. Experimental

### 2.1. Materials

Nanocomposites were made from montmorillonite (Cloisite 15A, dimethyldioctadecylammonium ions as surfactants, Southern Clay products, Gonzales, USA) and ε-polycaprolactone (Capa 6500, $M_w = 50{,}000$ g/mol, Solvay Interox Ltd, United Kingdom). Melt mixing was achieved in a co-rotating twin-screw mini-extruder (designed by DSM Research, The Netherlands) at 80 °C for 15 min at a mixing rate of 65 rotations/min and under nitrogen atmosphere. The MMT loadings were 1, 2, 4, and 10 wt%, respectively. A pure PCL sample was extruded as well for comparison.

### 2.2. X-ray scattering

X-ray scattering measurements were performed on the Dutch-Belgian Beamline (DUBBLE) at the European Synchrotron Radiation Facility (ESRF) in Grenoble, France. Two different measuring set-ups were used.

In the first set-up, the wavelength of the incident X-rays was 0.7294 Å and data were collected at room temperature for 5 min on a two-dimensional gas chamber SAXS-detector at 1.25 m from the sample position, covering the angular range $0.074 \leq s \leq 0.701$ nm$^{-1}$ (with $s = 2\sin\theta/\lambda$, $2\theta$ being the scattering angle and $\lambda$ the wavelength). After azimuthal averaging one-dimensional patterns were obtained. The scattering angles were calibrated using a silver behenate standard. These angles were converted to angles corresponding to Cu $K_\alpha$-radiation.

In the second set-up, time-resolved and simultaneous small-angle (SAXS) and wide-angle (WAXS) X-ray scattering experiments were conducted. The wavelength of the incident X-rays was 1.1273 Å. Scattered intensities were collected on a quadrant SAXS detector and a linear microstrip WAXS detector. The scattering angles were calibrated using silver behenate and collagen (SAXS) and silicon (WAXS). SAXS data were collected in the range $0.0355 \leq s \leq 0.174$ and WAXS data were collected over the angular range $7.7 \leq 2\theta \leq 66°$. Samples were inserted in copper ring holders and covered with aluminium foil. A Linkam hot stage was used for the temperature control. Samples were molten at a temperature of 100 °C for 2 min and then brought to the isothermal temperature of 47 °C, where data were collected for 40 min in subsequent time frames of 15 s. The WAXS and SAXS intensities were normalized to the intensity of the primary X-ray beam and corrected for the detector response.

### 2.3. Transmission electron microscopy (TEM)

Ultrathin sections were prepared on a Leica Ultracut ULT microtome, equipped with a Leica EM FCS cryo-unit. The samples were first trimmed with iron trimming knifes to trapezoidal shaped faces from which ultrathin sections (100 nm or less) were microtomed with a diamond knife (Drukker International) using −90 °C for the sample and −75 °C for the knife temperature. The thin sections were collected in water/dimethylsulfoxide (50:50) and finally deposited on copper TEM grids (square, 300 mesh). After drying on filter paper, TEM micrographs were made on a Philips CM10, operating at 80 kV.

### 2.4. Differential scanning calorimetry (DSC)

The Perkin–Elmer DSC 7 differential scanning calorimeter was calibrated with the melting point of indium (156.6 °C) and benzophenone (48.1 °C) for the temperature and with indium enthalpy (28.45 J/g) for the enthalpy.

In the dynamic DSC measurements, freshly extruded samples were kept 3 min at 100 °C and cooled at 10 °C/min to 10 °C. In the isothermal measurements, the cooling ramp was similar but was stopped at the isothermal temperature (42 and 47 °C), where the samples were allowed to crystallize isothermally. The exothermic crystallization heat was, after normalization to the PCL mass (not the sample mass, since the MMT mass contribution is irrelevant to the PCL crystallinity), converted to a PCL crystallinity using a reference $\Delta h_f$ value of 157 J/g for the melting of 100% crystalline PCL [25].

## 3. Data analysis

### 3.1. Small-angle X-ray scattering (SAXS)

An averaged melt pattern was subtracted as a background from the time-resolved SAXS patterns, collected using the second setup [17]. In this way the contribution to the scattering patterns by the morphology of (as will be shown below) intercalated silicates in the PCL matrix is effectively discarded. After a suitable extrapolation to zero and high angles linear correlation functions, $K(x)$, were calculated by cosine transformation and processed as described earlier [17] yielding

the long period, $L_p$, from the first side maximum in $K(x)$; the local volume fraction crystallinity in the PCL semicrystalline regions, $\phi_L$, from the so-called quadratic expression; the crystalline lamellar thickness, $l_c$, and the amorphous lamellar thickness, $l_a$, from the product of $L_p$ with $\phi_L$ or $(1-\phi_L)$, respectively. When using the quadratic expression independent information is needed to decide whether $\phi_L$ is associated with the minority or the majority fraction. Here the crystallinity values obtained from DSC are used as a guideline and $\phi_L$ was taken to be the minority phase over the full time range. The volume fraction of semicrystalline regions, $\alpha_S$, was calculated from the total scattering or invariant, $Q_{id}$, of the corresponding ideal two-phase structure, knowing the PCL crystalline, $\rho_c$, and amorphous, $\rho_a$, densities from the literature, $\phi_L$ and a scaling procedure [17,26]. For the crystalline and amorphous density, values of 1.2 and 1.02 g/cm$^3$ were taken, respectively [27,28]. In this procedure, it was assumed that $\alpha_S$ equals 1 at complete crystallization (which is after 40 min isothermal crystallization in the case of the nanocomposites). The product $\alpha_S\phi_L$ is a measure for the overall volume fraction crystallinity ($\chi_v$). Using the mass densities of the amorphous and crystalline phases, this volume fraction crystallinity was transformed into a mass fraction crystallinity $\chi_m$ for comparison with the DSC mass fraction crystallinity [17]. It has to be noted that the crystallization of pure PCL was not finished after 40 min isothermal crystallization. Therefore, this sample was cooled down to room temperature after the isothermal crystallization to ensure complete crystallization and an $\alpha_S$ value equal to 1. The data related to the cooling run are not discussed in this paper but were used in the scaling procedure. Accordingly, it was found that $\alpha_S$ after 40 min of PCL crystallization at 47 °C only reaches 0.45.

### 3.2. Wide-angle X-ray scattering (WAXS)

A linear background was subtracted from the WAXS data. In this particular angular range the contribution of the silicate layers to the patterns is negligibly small. The WAXS pattern evolution of pure PCL during it's crystallization is shown in Fig. 1. The peaks around 21 and 22 ° are from the 110 and 111 reflections, respectively [24]. The peak around 24° corresponds to the 200 reflection. The patterns were fitted to the sum of a Lorentz function for the amorphous halo and a Pearson function for each crystalline peak, using the Microcal™ Origin® data processing program [17]. Reliable crystallinities could not be calculated because of uncertainties in the background that strongly affect the amorphous halo contribution. Therefore, a crystallinity index is reported, which is the total integrated intensity of all crystalline peaks normalized to the total integrated intensity of these peaks at full crystallization (which for pure PCL was only reached after cooling to room temperature, see Section 3.1). The lateral dimension of the crystallites related to the 110 reflection, $D_{110}$, was estimated from the peak width at half height and applying Sherrer's equation [17,29].

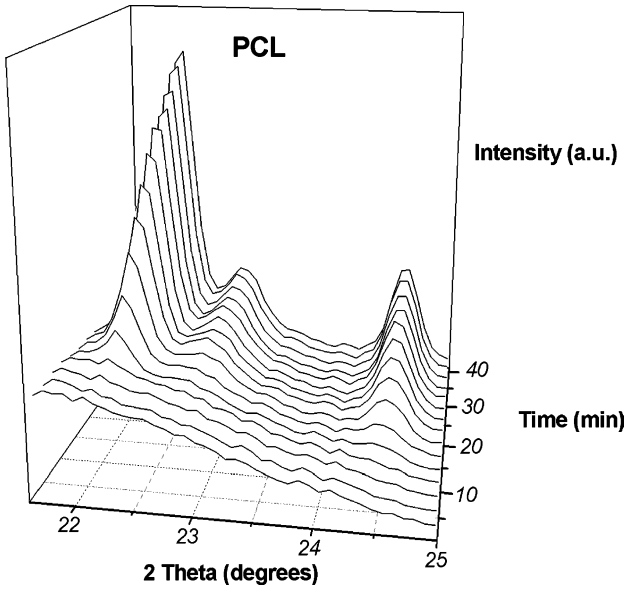


Fig. 1. WAXD patterns of pure PCL measured during isothermal crystallization at 47 °C. For clarity only one scattering pattern in 10 is displayed.

## 4. Results and discussion

### 4.1. Nanocomposite morphology

Fig. 2 shows the SAXS curves (set-up 1) of pure MMT, pure PCL and the PCL/MMT nanocomposites with 1, 2, 4 and 10 wt% MMT. The SAXS curve of pure (surfactant modified) MMT shows a strong peak at $2\theta = 2.8°$, corresponding to the interlayer distance of the silicate layer stacks, i.e. 32 Å. The PCL/MMT nanocomposites show peaks at $2\theta = 2.3°$, corresponding to an interlayer distance of 38 Å. The increase in interlayer distance points to the intercalation of polymer chains between the silicate layers. The peaks corresponding to the PCL/MMT nanocomposites are also sharper than the pure clay peak and a clear second order reflection appears, which indicates a narrowing of the interlayer distance distribution upon the insertion of polymer chains. This can either be due to a true equalization of the original clay galleries that are initially

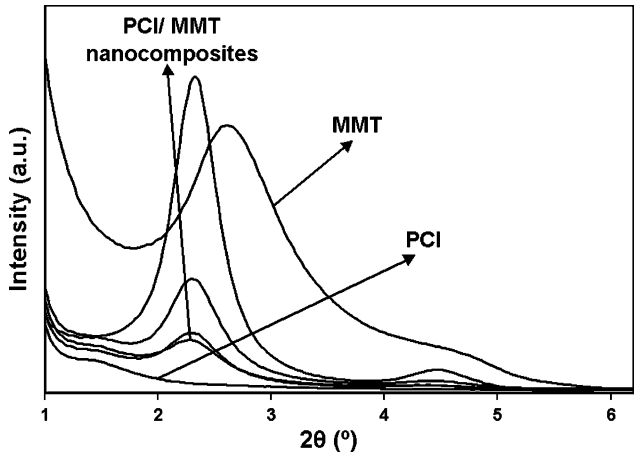


Fig. 2. X-ray scattering patterns of PCL and PCL/MMT nanocomposites at room temperature.

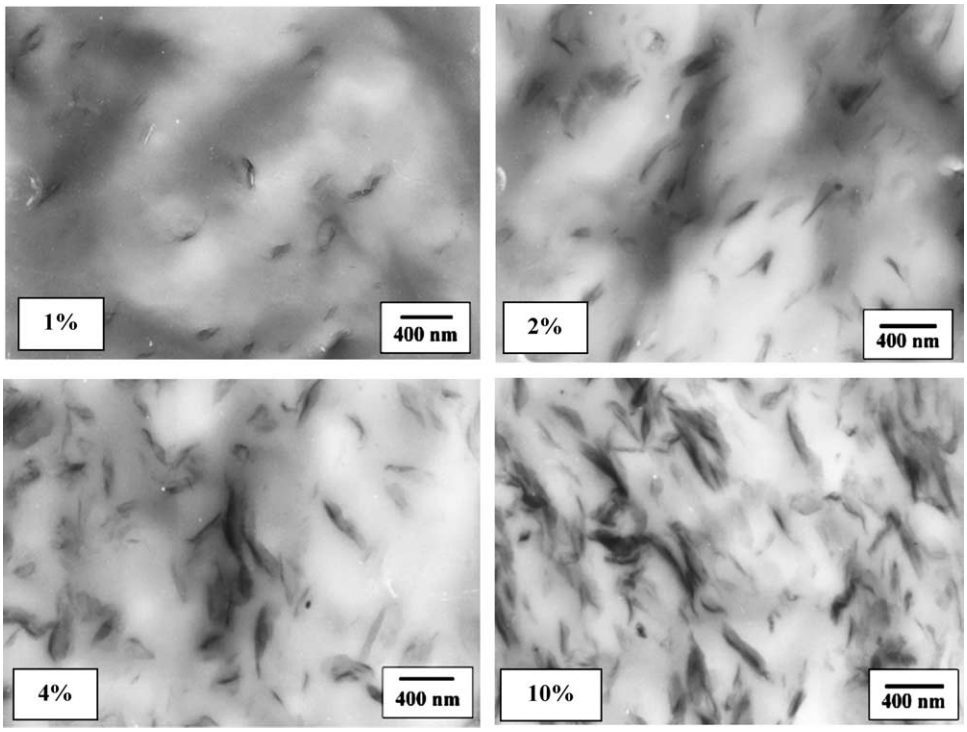


Fig. 3. Transmission electron micrographs of PCL and its MMT composites at the indicated MMT concentrations.

unequally surfactant swollen or alternatively to the selective full detachment of a given inter layer distance population (likely the most swollen one) by which the distribution in the remaining stacks narrows. Whatever, the case the fact that a sharp reflection is observed, excludes the option of a full exfoliation, which is confirmed by TEM.

In Fig. 3, the TEM micrographs of PCL + 1% MMT, PCL + 2% MMT, PCL + 4% MMT and PCL + 10% MMT are shown. The observed black lines cannot be interpreted as individual silicate layers as they are too large and thick. The size and shape of the lines in the micrographs thus supports the view of intercalated stacks. Although this MMT/surfactant/polymer/processing combination does not allow for a full exfoliation it cannot be denied that the surfactant has been effective! For comparison, a TEM micrograph of PCL with 8% unmodified cloisite $Na^+$ is shown in Fig. 4. This cloisite type MMT without surfactants cannot be intercalated and the original MMT stack morphology is fully preserved even after mixing with PCL. These clay aggregates are larger, less diffuse and darker compared shape to the intercalated, and most likely partially broken-up stacks seen in Fig. 3.

### 4.2. DSC crystallization behavior

Fig. 5 displays the dynamic, respectively, isothermal crystallization curves for pure PCL and the PCL/MMT nanocomposites. The curves are shifted vertically for clarity.

In the dynamic crystallization curves (Fig. 5(a)), the crystallization onset temperature increases with increasing MMT content. The crystallization peak temperature first increases with increasing MMT content till 4% MMT and then decreases for higher MMT contents. The exothermic peak of PCL + 10% MMT is clearly broader, pointing at a decreased overall crystallization rate.

The trends observed in the dynamic experiments are confirmed in the isothermal crystallization curves at 42 °C displayed in Fig. 5(b). The crystallization onset time decreases with increasing MMT content. The crystallization half-time decreases with increasing MMT content, but increases somewhat for PCL + 10% MMT. Similarly, the overall crystallization time decreases with increasing MMT content till 4% MMT but increases again for PCL + 10% MMT.

It is clear from the increase in the crystallization onset temperature in the dynamic DSC measurement and the decrease in crystallization onset time in the isothermal DSC measurements that the silicate layers act as nucleating agents

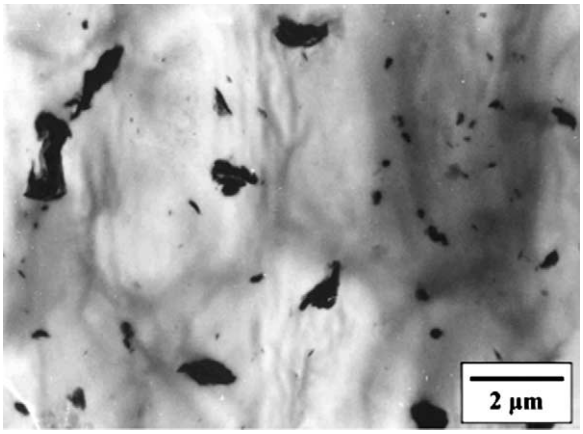


Fig. 4. Transmission electron micrographs of PCL + 8% MMT composite (cloisite type MMT without surfactant).

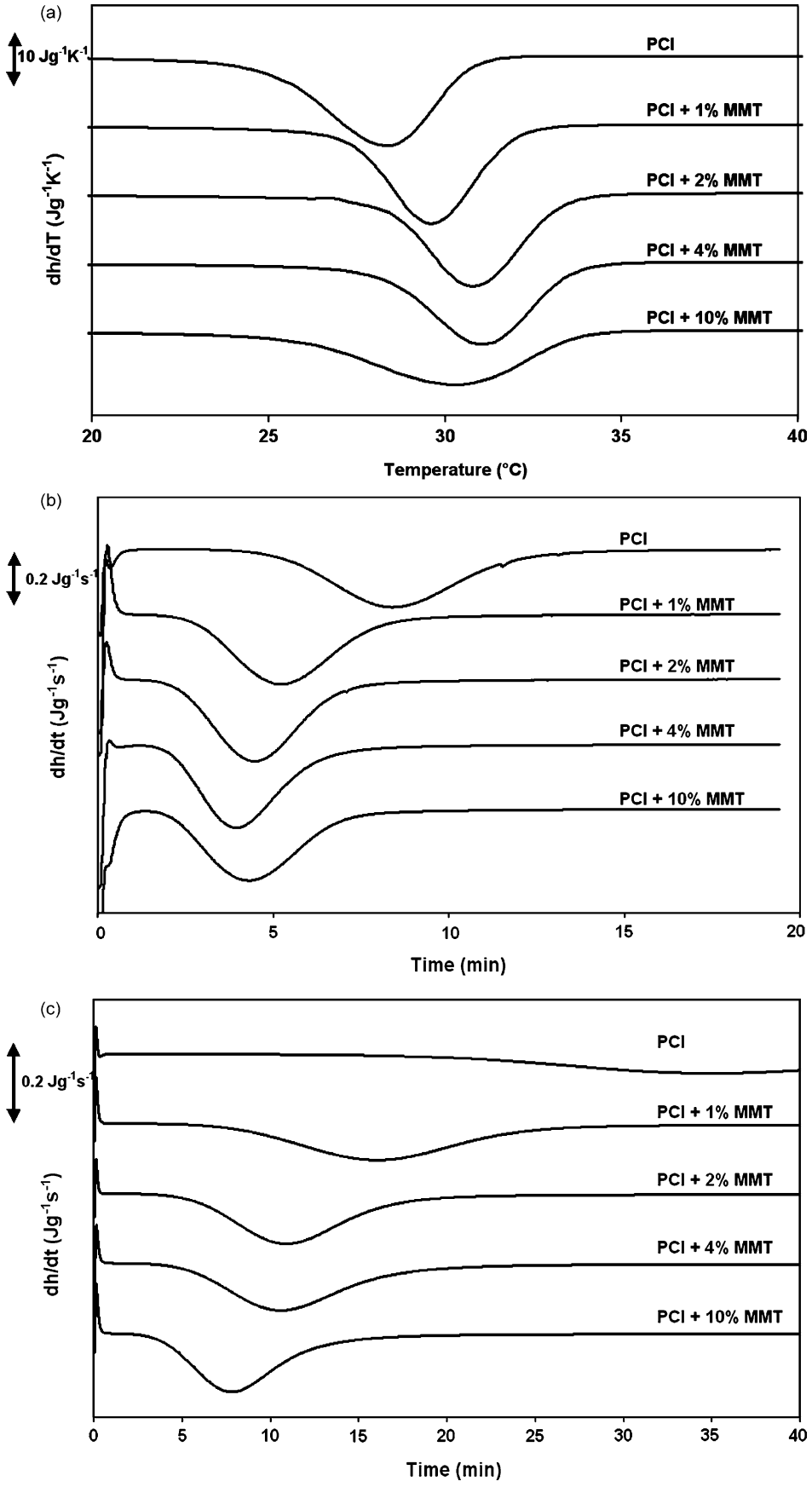


Fig. 5. Dynamic (a) and isothermal (b) and (c) DSC crystallization curves of PCL and PCL/MMT nanocomposites. The cooling rate was 10 °C/min and the isothermal crystallization temperatures 42 °C (b) and 47 °C (c).

for the PCL crystallization. However, at large MMT concentration (10%) a decrease in the overall crystallization rate is observed. The overall crystallization rate is proportional to both the primary nucleation rate and the crystal/spherulite growth. Since irrespective of the MMT amount one observes an earlier crystallization onset, one has to accept that primary nucleation is enhanced in all cases. Accordingly, the decrease in overall crystallization rate has to be associated with a decrease in crystal/spherulite growth rate, caused by a disturbance of the silicate layers. Such a decrease could microscopically be registered in the case of intercalated PEO nanocomposites [17]. Unfortunately, in the present case the PCL spherulites are too small and imperfect for microscopy or light scattering experiments, independent of the MMT amount. The similarity in the DSC data is, however, striking and points at a similar behavior. The slightly lower crystallinity for the nanocomposites serves as an additional argument in favor of this disturbance of the crystal growth. Because enhanced primary nucleation and retarded crystal growth have an opposite effect on the overall crystallization rate, one observes a maximum in the overall crystallization rate at PCL + 4 wt% MMT. At lower MMT concentrations, enhanced nucleation dominates, while at the highest MMT concentration the growth retarding effect becomes apparent. A similar crystallization behavior was observed for PEO/MMT and PA-6/MMT nanocomposites and explained as mentioned in the introduction [17,20–22].

The isothermal crystallization curves at 47 °C displayed in Fig. 5(c), show a slightly different behavior. The crystallization onset time decreases with increasing MMT content and the crystallization half-time and overall crystallization time decrease with increasing MMT content just like for crystallization at 42 °C. However, this trend in the crystallization half time does not alter for PCL + 10% MMT in contrast to when crystallized isothermally at 42 °C. Apparently, a sufficiently high degree of supercooling is needed for a disturbed crystal growth. At 47 °C, the crystal growth rates are low compared to at 42 °C but at 47 °C, the rate for a migration of the disturbing

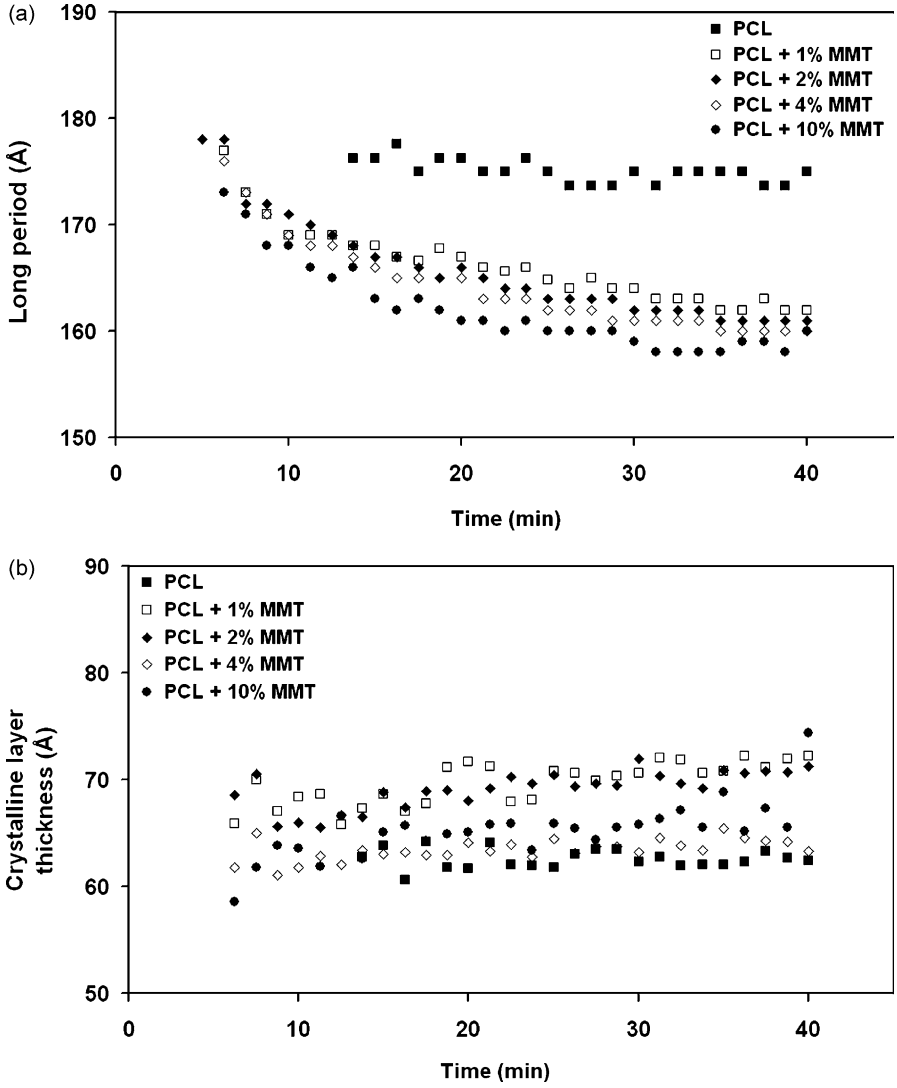


Fig. 6. The long period (a), crystalline layer thickness (b), amorphous layer thickness (c) and the volume fraction semicrystalline material (d) of pure PCL and the PCL/MMT nanocomposites as a function of time during isothermal crystallization at 47 °C. For clarity only one measurement point out of five has been drawn.

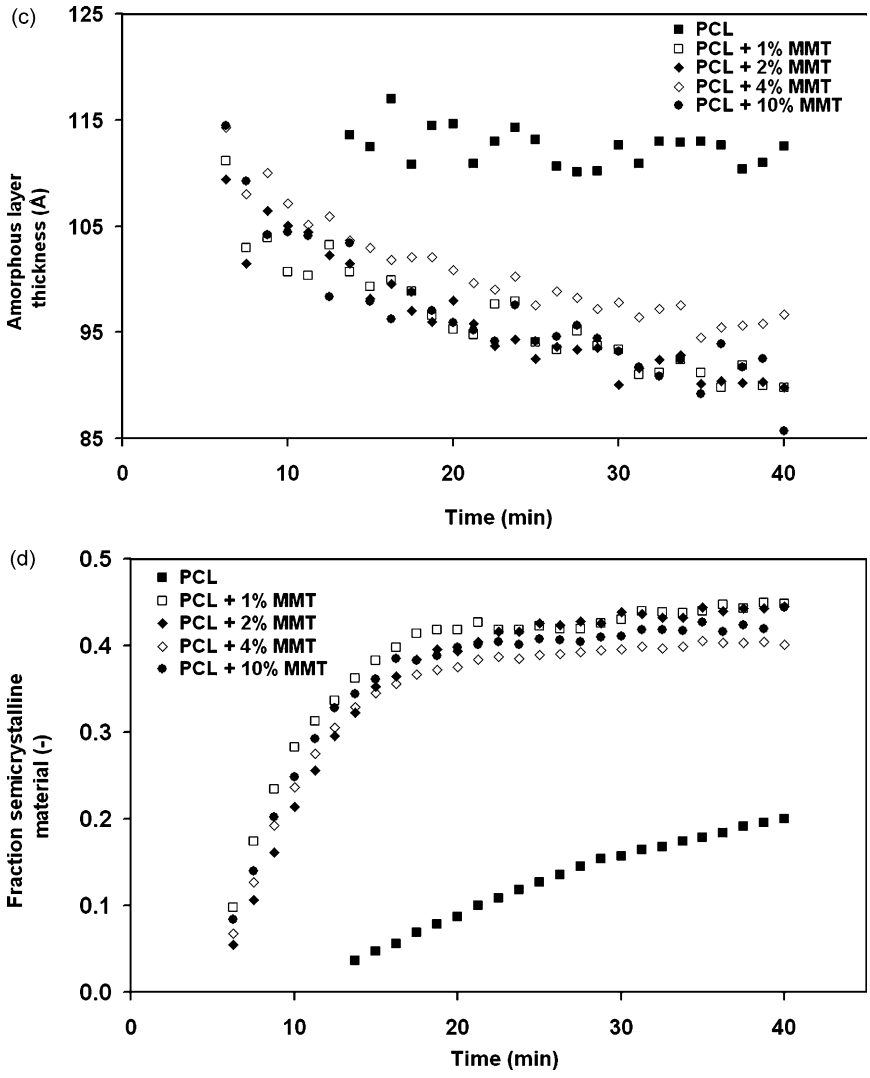


Fig. 6 (*continued*)

silicate obstacles away from the crystal growth fronts and the diffusion of the PCL molecules towards the growth fronts for sure is higher. As a result crystallization is the rate limiting step at 47 °C whereas at 42 °C (or at high supercooling in general) this is—at least for 10% MMT—opposite. The overall crystallinity, obtained from the integrated DSC peak areas for crystallization at 47 °C and corrected for the PCL concentration in the samples, is 37% for PCL and around 36% for the PCL/MMT nanocomposites.

### *4.3. Semicrystalline structure development*

#### *4.3.1. SAXS*

The evolution of the long period, the crystalline and amorphous layer thicknesses and the SAXS based volume fraction semicrystalline material with time, is given in the Fig. 6(a)–(d), respectively. From Fig. 6(d), it can be derived that the crystallization onset occurs earlier and that the overall crystallization time is shorter for the PCL/MMT nanocomposites compared to pure PCL. This confirms the DSC measurements and the notion that the silicate layers act as nucleating agents for the crystallization of PCL but that the silicate migration and PCL diffusion rates are sufficiently high not to result in any retardation. The slow crystallization rate at 47 °C was selected deliberately for X-rays characterization in order to allow for longer data acquisition times during the course of crystallization. At 47 °C the crystallization of pure PCL is particularly slow and not complete after 40 min as mentioned in Section 2.

To our opinion there is no significant time evolution in the $l_c$ values, nor there is a difference between the different samples, pure PCL included. The small observed fluctuations might very well be related to the background subtraction procedure, which is rather involving. The high angle tail of the scattering patterns is affected in particular and as a result so is the autocorrelation triangle in $K(x)$ from which $\phi_L$ and hence $l_c$ are derived [17,26]. In contrast, $L_p$ is not affected by the background subtraction procedure and fully reliable. Even if the fluctuations in $l_c$ were true, they would be small compared to the evolution in $L_p$.

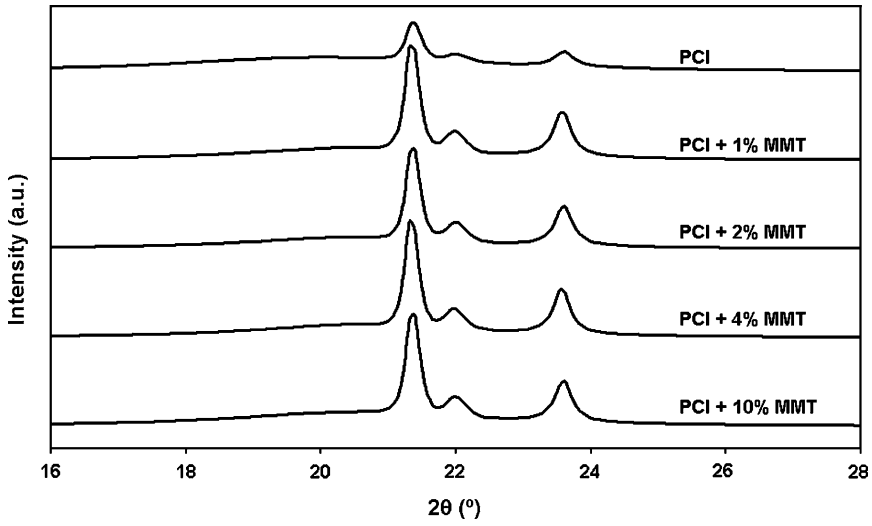


Fig. 7. WAXD curves of PCL and PCL/MMT nanocomposites at the end of isothermal crystallization at 47 °C.

Accordingly, the (reliable) dominant evolution in $L_p$ is a reflection of the genuine evolution in $l_a$.

All nanocomposites display a pronounced decrease in $l_a$ with time, which is a signature of secondary crystallization via the insertion of new crystals in between already existing ones. At first sight such a process is absent in pure PCL, but this is deceptive! Obviously, secondary crystallization follows primary crystallization. In this context, primary crystallization is defined as the growth of spherulites, involving primary crystals in rather open 'primary stacks'. Behind the primary spherulite growth front another one follows much slower, involving the further conversion of amorphous material that was left amorphous in the primary stacks by the insertion of new crystals. The strong upswing in the overall crystallinity (Fig. 6(d)) of the composites reflects a strong increase in $\alpha_S$, reaching unity after about 15 min. Due to the high amount of primary nuclei, space is rapidly filled with primary crystals. Since secondary crystallization is slow, the amount of secondary crystals is rather low at this moment in time. Accordingly, the entire volume simultaneously is subject to secondary crystallization, as is observed in the decrease in $l_a$. In contrast, the space in pure PCL is filled with primary stacks only slowly, due to the lack of primary nuclei. After 40 min only 45% of the volume is filled with stacks/spherulites. At any moment in time during the present experiment new primary stacks are formed, either at the front of growing spherulites or at the creation of new spherulites (by heterogeneous nucleation on foreign substances in PCL that are less active than the mineral layer stacks). After a given time, secondary crystallization follows just like in the composite case, but at any particular moment in time both primary and secondary stacks are present, resulting in a less well-defined signature of secondary crystallization in SAXS. There is only a slow decrease in $L_p$ and $l_a$, due to a superposition of primary stacks

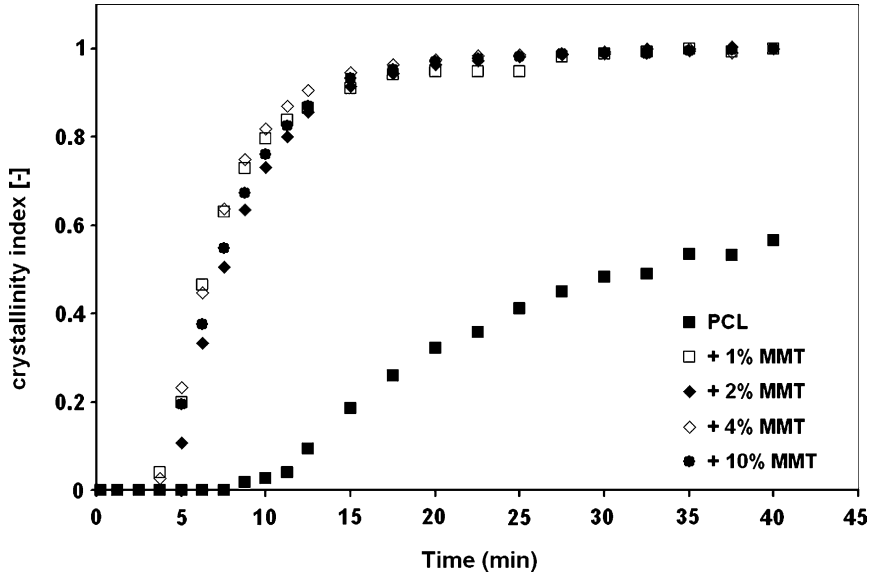


Fig. 8. Crystallinity indexes of pure PCL and PCL/MMT nanocomposites as a function of time during isothermal crystallization at 47 °C.

and a multitude of secondary stacks at different stages of their development. The PCL structural parameters at the onset of crystallization are identical to those at the onset of crystallization in the nanocomposites since here in both cases only primary stacks are present. This resemblance—in particular—is taken as evidence for the structural similarity of PCL in its pure form and in the nanocomposites.

The PCL local crystallinity, $\phi_L$, after 40 min is only 34% whereas the composites already reached 42%. The latter value is also a measure for the overall crystallinity since for these samples $\alpha_S = 1$ at the end of the isothermal segment. The difference between the DSC and SAXS crystallinity for pure PCL disappears when PCL is cooled to room temperature due to further primary (increase in $\alpha_S$) and secondary (increase in $\phi_L$) crystallization. The SAXS volume fraction crystallinity, $\chi_v$, values reached at the end of the crystallization, have been converted to mass fraction crystallinity, $\chi_m$, values (Section 3.1). The SAXS overall mass fraction crystallinity is 48% for PCL and around 45% for the PCL/MMT nanocomposites. The SAXS overall crystallinities are considerably higher than the DSC crystallinities, which can be due to the contribution in SAXS of crystalline–amorphous transition layers [30] or dense rigid amorphous material in between the lamellar crystal grains [31]. However, the SAXS overall mass fraction crystallinities are close enough to those of DSC to justify the assumption that $\phi_L$ is associated with the minority component (Section 3.1).

#### *4.3.2. WAXS*

The WAXS patterns obtained after 40 min of isothermal crystallization of pure PCL and the PCL/MMT nanocomposites are given in Fig. 7 and are hardly different except for the lower intensity of the crystalline peaks in the pattern of pure PCL. The peak widths too are—within experimental error—identical for all samples and yield Debye–Sherrer crystal sizes of about 350 Å ($D_{110}$). The evolution of the crystallinity index during crystallization is represented in Fig. 8 and qualitatively resembles the SAXS based crystallinity evolution in Fig. 6(d), as expected.

## 5. Conclusions

The combination of surfactant modified MMT, PCL and the adopted melt processing procedure results in intercalated nanocomposites. The silicate layers clearly act as nucleating agents for the crystallization of the PCL matrix, resulting in an increase in the overall crystallization rate. However, at a sufficiently high MMT concentration and degree of supercooling the polymer swollen silicate layer stacks disturb crystal growth by which the overall crystallization rate decreases. Whether the silicate layers act as crystallization roadblocks or whether they hinder polymer chain motion cannot be derived from the present data set.

In any case, the observed changes in the crystallization behavior of the PCL matrix are very similar to those in intercalated PEO/MMT nanocomposites [17] and exfoliated PA-6/MMT nanocomposites [20–23]. It seems a general rule that the addition of low MMT quantities results in an increase in nucleating sites and an inflation of the overall crystallization rate but that—when the MMT concentration is sufficiently high to hinder the process of crystal growth—this trend is reversed. Further studies are needed to learn whether or not a sufficiently high degree of supercooling is a necessary requirement in general for the occurrence of the retarding effect. For sure this condition is needed in the case of a PCL matrix and an MMT contents of 10 wt%.

In the present case of PCL, and when the retarding effect is absent, one cannot detect any difference in final semicrystalline structure between pure PCL and its nanocomposites. The poorer nucleation in the case of pure PCL, however, results in a time wise smearing of primary and secondary crystallization whereas in the nanocomposites these event are well separated due to a nucleation induced, efficient and rapid primary crystallization.

## Acknowledgements

The authors would like to thank the Fund for Scientific Research—Flanders (Belgium) as well as the Research Council KULeuven for the financial support for this research; one of them (B.G.) is a postdoctoral fellow of the Fund for Scientific Research—Flanders. The authors also would like to acknowledge the Dutch-Belgian beamline (DUBBLE) research group at the ESRF, Grenoble, France, for their help and support with the time-resolved small angle X-ray experiments.

## References

[1] Alexandre M, Dubois P. Mater Sci Eng 2000;28(1–2):1–63.
[2] Giannelis EP, Krishnamoorti R, Manias E. Adv Polym Sci 1999;138:107–47.
[3] Lincoln DM, Vaia RA, Wang Z-G, Hsiao BS. Polymer 2001;42:1621–31.
[4] Lepoittevin B, Devalckenaere M, Pantoustier N, Alexandre M, Kubies D, Calberg C, et al. Polymer 2002;43(14):4017–23.
[5] Pantoustier N, Lepoittevin B, Alexandre M, Kubies D, Calberg C, Jerome R, et al. Polym Eng Sci 2002;42(9):1928–37.
[6] Maiti P, Nam PH, Okamoto M, Hasegawa N, Usuki A. Macromolecules 2002;35:2042–9.
[7] Moussaif N, Groeninckx G. Polymer 2003;44:7899–906.
[8] Wu TM, Chen EC. Polym Eng Sci 2002;42(6):1141–9.
[9] Wu TM, Wu JY. J Macromol Sci, Phys 2002;B41(1):17–31.
[10] Maiti P, Nam PH, Okamoto M, Kotaka T, Hasegawa N, Usuki A. Polym Eng Sci 2002;42(9):1864–71.
[11] Kamal MR, Borse NK, Garcia-Rejon A. Polym Eng Sci 2002;42(9):1883–96.
[12] Liu X, Wu Q. Polymer 2002;43:1933–6.
[13] Liu X, Wu Q. Eur Polym J 2002;38:1383–9.
[14] Medellin-Rodriguez FJ, Burger C, Hsiao BS, Chu B, Vaia RA, Phillips S. Polymer 2001;42:9015–23.
[15] Lincoln DM, Vaia RA, Wang ZG, Hsiao BS, Krishnamoorti R. Polymer 2001;42:9975–85.
[16] Xu W, Ge M, He P. J Polym Sci, Part B: Polym Phys 2002;40:408–14.
[17] Homminga DS, Goderis B, Dolbnya I, Reynaers H, Groeninckx G. Crystallization behavior of polymer/montmorillonite nanocomposites. Part I. Intercalated poly(ethylene oxide)/montmorillonite nanocomposites. 2005;46:11359–65.

[18] Wunderlich B. Macromolecular physics, vol. 2. New York: Academic Press; 1976 [chapter 5].
[19] Groeninckx G, Berghmans H, Overbergh N, Smets G. J Polym Sci, Polym Phys Ed 1974;12:303–16.
[20] Fornes TD, Paul DR. Polymer 2003;44:3945–61.
[21] Van Es M, Polymer–clay nanocomposites. Doctoral Thesis. The Netherlands: Technical University of Delft, ISBN 90 77017 27 5; 2001 [chapter 7].
[22] Homminga DS, Goderis B, Mathot VBF, Groeninckx G. Crystallization behavior of polymer/montmorillonite nanocomposites. Part III. Polyamide-6/montmorillonite nanocomposites, influence of matrix molecular weight, and of montmorillonite type and concentration Polymer (in press) doi:10.1016/j.polymer.2005.10.141.
[23] Jimenez G, Ogata N, Kawai H, Ogihara T. J Appl Polym Sci 1997;64(11): 2211–20.
[24] Messersmith PB, Gianellis EP. J Polym Sci, Part A: Polym Chem 1995; 33:1047–57.
[25] Athas Databank, URL: http://web.utk.edu/~athas/databank/intro.html, last revision February 5; 2000.
[26] Goderis B, Reynaers H, Koch MHJ, Mathot VBF. J Polym Sci, Part B: Polym Phys 1999;37:1715–38.
[27] Hayashi T, Nakayama K, Mochizuki M, Masuda T. Pure Appl Chem 2002;74(5):869–80.
[28] Chatani Y, Okita Y, Tadokoro H, Yamashita Y. Polym J 1970;1:555–62.
[29] Alexander LE. X-ray diffraction methods in polymer science. Hunington, NY: Robert E. Krieger Publishing Company; 1979 p. 423.
[30] Goderis B, Reynaers H, Koch MHJ. Macromolecules 2002;35(15): 5840–53.
[31] Goderis B, Klein PG, Hill SP, Koning CE. Prog. Colloid Polym Sci 2005;130:1–11.